Wavelet Modeling of the Gravity Field over Japan

Isabelle PANET[1,2], Yuki KUROISHI[2], Matthias HOLSCHNEIDER[3]

Abstract

Knowing the geoid over Japan is essential for many geodetical and geophysical applications. Because of the tectonic settings of the area, significant geoid undulations occur in a wide range of spatial scales and make the determination of the geoid a complex task. In some applications, high absolute accuracy at long and medium wavelengths is required for geoid models with high resolution, which can be achieved by a proper combination of satellite gravity information with densely-distributed surface gravity data after careful consideration of their respective error characteristics. Here we show how to realize such a combination in a flexible way using spherical wavelets. The gravity potential is expressed as a linear combination of wavelets, whose coefficients are obtained by a least squares adjustment of the datasets. The combination needs to handle a large system of equations and we apply a domain decomposition method. First, we define sub-domains as subsets of wavelets. Based on the localization properties of the wavelets in space and frequency, we define hierarchical sub-domains of wavelets at different scales. On each scale, blocks of sub-domains are defined by using a tailored spatial splitting of the area. Second, we approximate the normal matrix for each block by introducing local approximation of the wavelets depending on the scale, in which local averages of the data are actually used for computation. Finally, we solve the system iteratively. In the beginning we validate the method with synthetic data, considering two kinds of noise: white noise and colored noise. We then apply the method to data over Japan: a satellite-based geopotential model, EIGEN-GL04S, and a local gravity model from a combination of land and marine gravity data and an altimetry-derived marine gravity model. A hybrid spherical harmonics/wavelet model of the geoid is obtained at about 15 km resolution and the residuals indicate the existence of possible biases in the surface model. This information is used to correct the local model and the method is repeated with the corrected data, resulting in an improved hybrid model of the gravity field over Japan.

1. Introduction

Knowing the geoid over Japan in detail is essential for many applications. First, conversion between GPS-derived and leveled heights becomes possible with knowledge of the geoid. It allows us to monitor crustal movements over long periods of time beyond the advent of GPS, and thus to better understand crustal activities during the seismic cycle in Japan. Moreover, the geoid gives us a reference surface for ocean dynamics. An absolute geoid model with a sufficient accuracy can yield the absolute amount of ocean currents, leading to a better understanding of the Kuroshio Current.

The geoid is defined as the equipotential surface of the gravity field corresponding to the mean sea surface and an accurate gravity model, if available, can be used to determine the geoid accurately. Because of the tectonic settings in and around Japan, located in a trench and island arc region where four tectonic plates converge, significant undulations of the gravity field and accordingly the geoid occur over a wide range of spatial scales and make the determination of the geoid a complex task.

The emergence of dedicated-gravity satellite missions such as GRACE (launched in 2002) and GOCE (planned for launch in March 2009) greatly improves the accuracy of the geoid model at long and medium wavelengths. These missions provide a global coverage of gravity field information with a high absolute accuracy in uniform fashion, to spatial resolutions of about 200 km for GRACE and 100 km for GOCE.

Merging the data obtained by these missions with dense surface gravity data (land, marine and altimetric data) allows us to highlight possible biases of the surface data at larger scales and thus to improve the quality of the surface data and consequently of a resulting geoid model. Different types of gravity field datasets can be combined in a very flexible way by using a functional representation of the

[1]Institut de Physique du Globe de Paris, France, [2]Geographical Survey Institute, Space Geodesy Research Division, Tsukuba, Japan, [3]University of Potsdam, Department of Applied Mathematics, Potsdam, Germany

gravity field based on spherical wavelets.

In this paper, we first describe how to compute a wavelet model of the gravity field, applying iterative algorithms to handle a large system of equations. Then, we validate our approach with synthetic data. Finally, we apply the method to data over Japan.

2. Wavelet representation of the gravity field

2.1 Wavelet frames

Wavelets are functions localized in both space and frequency. They have been extensively described in the literature (for instance, Holschneider (1995) and Mallat (2000)). Wavelet theory has been extended to spherical geometry for Earth sciences applications (Freeden *et al.*, 1998; Holschneider *et al.*, 2003). Here we use Poisson multipole wavelets on the sphere, following Holschneider *et al.* (2003). Because those wavelets can be identified as equivalent multipolar sources of gravity within the Earth, they are well suited to represent the potential field of the Earth's gravity. A wavelet family is constructed with two parameters: a scale parameter (defining the spatial extent), and a position parameter (defining the location). Fig. 1 shows two examples of such wavelets on the sphere having large and small scale parameters.

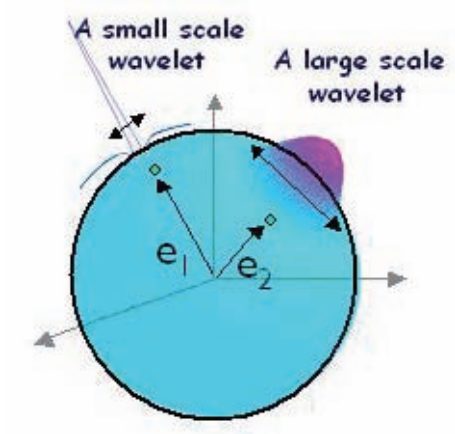

Fig. 1 Two Poisson multipole wavelets of order 3 on the sphere.

The Earth's gravity potential can be represented as a linear combination of wavelets properly sampled in scale and position. We construct a family of multipole wavelets of order 3, following Chambodut *et al.* (2005) and Panet *et al.* (2006).

A selection of scales should be made in order to provide a regular coverage of spectrum. Because the sphere is bounded, the wavelets at different scales are not truly dilated versions of each other. However, they behave so when the scale becomes small. On a given scale, all wavelets are rotated copies of each other.

Regarding the position parameter, wavelets are sampled with their central locations at the vertices of a spherical mesh. The number of wavelets must increase as the scale decreases, because the dimension of the harmonic spaces to generate increases. The spherical meshes therefore become finer as the scale decreases. The mesh on each scale should be chosen so that the wavelets have as regular coverage of the sphere as possible. For local modeling applications, the target area is limited and we may build simple meshes whose vertices are sampled regularly in longitude and latitude.

A family of wavelets thus sampled forms a frame; its representation may be redundant. The frame (over-) completeness can be estimated by approximating the wavelets to band-limited functions and by comparing the number of wavelets approximated in different wavelength bands with the dimensions of the corresponding harmonic spaces (Holschneider *et al.*, 2003). Panet *et al.* (2004) and Chambodut *et al.* (2005) discuss the spectral coverage of this family of wavelets and show that our selection (described in detail later in section 4.1) is over-complete at an estimated redundancy of 1.4 to a spatial resolution of 10 km.

2.2 Consideration for application to local gravity field modeling

We should make some special consideration for applications to local gravity field modeling. Various kinds of data, with different spatial coverage and different error characteristics, are to be combined. Among them are gravity anomalies measured locally on the Earth's surface and measurements on board satellites at the altitude of the satellite orbits. In the following, we presuppose that there are two data sets available: a set of local high-resolution gravity anomalies and a global geopotential model expanded in spherical harmonics complete to degree and order 120, from dedicated-gravity satellite missions. From the latter we compute and use as a second set of data geopotential values

at the ground level in the area considered. Since the geopotential model contains much more reliable signals at longer wavelengths than local gravity anomaly data, we extend the data area of geopotential values by two degrees in each of four directions (north, south, east and west) as compared to the gravity anomaly data coverage.

Wavelengths longer than the extent of the data coverage will not be reliably recovered from local data and we use solely the global geopotential model at its lower frequency parts in the resulting model. Then, in the gravity field modeling, we take data residuals from the lower parts of the geopotential model and combine them by a wavelet-based method. In the representation of the residual gravity field, therefore, we should include wavelets at scales no larger than a half of the computation area size. To better constrain the wavelet coefficients from local data, we limit wavelets to scales no larger than about a fourth of the area width.

2.3 Computation of wavelet coefficients

A least-squares inversion of the datasets is applied to computation of the wavelet coefficients. Since the gravity potential is written as a linear combination of wavelets, the observation equations for each dataset, i, are derived from the functional relation between the data type and the gravity potential. In matrix notations, this reads $A_i \cdot x = b_i$, where b_i is the measurement vector, A_i the design matrix, and x the coefficients to be determined. This leads to the normal equations: for a dataset, i, we have $N_i \cdot x = f_i$, where $N_i = A_i^t \cdot W_i \cdot A_i$ is the normal matrix, W_i is the weight matrix based on the supposed measurement noise, and $f_i = A_i^t \cdot W_i \cdot b_i$ is the associated right hand side. The normal equations are summed up for all datasets to form the global system and a regularization matrix, K is added with a parameter, λ :

$$(N + \lambda K) \cdot x = f$$

with $N = \sum_i N_i$ and $f = \sum_i f_i$. The size of the normal equation system is $N_w \times N_w$, where N_w is the total number of wavelets. We denote $G = N + \lambda K$ the regularized normal matrix.

The regularization is introduced for two reasons. First, the characteristics of the measurements lead to an ill-posed problem. Physical a-priori information may be needed to define the regularization matrix. Usually a condition expressing the spectral decrease of the field's energy is used (Chambodut *et al.*, 2005; Panet *et al.*, 2004). In the case of satellite data handling, the ill-posedness in the downward continuation may be regularized by the use of a surface dataset. Second, if the wavelets form a frame, there exists no unique solution, x to the problem because of the redundancy of the representation. In such cases, one has to add a purely numerical regularization, for instance, a Tikhonov regularization, to impose a unique solution. This numerical regularization, however, will interfere with the physical one.

3. Domain decomposition methods

3.1 Definition of the sub-domains

To solve the large system of equations, we use an iterative approach together with data compression, following domain decomposition methods. The interested reader may refer to Chan and Mathew (1994) and Xu (1992) for a detailed presentation of domain decomposition algorithms. We recall here the main principles.

Let us introduce the space $H = L^2(\Sigma)$ generated by the wavelet family, where Σ is the mean Earth sphere. When we compute a wavelet model by the least-squares adjustment of data, we actually project the data on H. We may split this space H into smaller non-overlapping sub-spaces $\{H_{\{i,0\}};\ i=1,...,p\}$, called sub-domains, so that we have: $H = \sum_{i=1}^{p} H_{\{i,0\}}$. The sub-domains are spaces generated by subsets of wavelets and, by taking advantage of the good localization of the wavelets in space and frequency we define our sub-domains in the following way.

We first split H into non-overlapping sub-spaces $\{H_{\{ai,0\}};\ i=1, ..., N_{scales}\}$, where $H_{\{ai,0\}}$ is made by all wavelets on scale a_i; we refer to them as scale sub-domains. If sub-domain $H_{\{ai,0\}}$ is still composed of a large number of wavelets, we split it again into non-overlapping sub-domains of smaller size $\{H_{\{ai,0\}\{j,0\}};\ j = 1, ..., N_{blocks(i)}\}$. These sub-domains are generated by subsets of wavelets at scale a_i, and their union corresponds to space $H_{\{ai,0\}}$:

$$H_{\{ai,0\}} = \cup_{j=1}^{Nblocks(i)} H_{\{ai,0\}\{j,0\}}.$$

They are referred to as block sub-domains. To be general, let us assume that all scale sub-domains have a block sub-domain splitting. We regard $N_{blocks(i)} = 1$ if there is only one block. The number of blocks may vary depending on the scale and one can split space H so that sub-space $H_{\{ai,0\}\{j,0\}}$ is generated by a not too large number of wavelets (no more than a few thousands).

We may also define an overlapping splitting of sub-space $H_{\{ai,0\}}$ as made of a set of overlapping blocks $\{H_{\{ai,0\}\{j,\delta(i)\}};\ j = 1, ..., N_{blocks(i)}\}$. Overlapping blocks $H_{\{ai,0\}\{j,\delta(i)\}}$ are obtained by augmenting non-overlapping blocks $H_{\{ai,0\}\{j,0\}}$ with wavelets located in overlap areas of width $\delta(i)$. The size of the overlap area $\delta(i)$ obviously depends on the scale a_i. However, for simplicity of notation, we will refer to it as δ here. It is also possible to define a set of overlapping scale sub-domains, by extending sub-domain $H_{\{ai,0\}}$ with the wavelets on adjacent scales a_{i-1} or a_{i+1}. Let us note $n_{\{ai,0\}\{j,\delta\}}$ the number of wavelets that generate $H_{\{ai,0\}\{j,\delta\}}$.

Let us now introduce the projection and extension operators between H and the sub-domains. In the following, we will work in the space of wavelet coefficients $l^2(\Gamma)$, where $l^2(\Gamma) = \{ x;\ ||x^2|| = \sum_{n\in\Gamma} |x[n]|^2 < +\infty \}$ and identify sub-domains $H_{\{ai,0\}\{j,\delta\}}$ with subsets of wavelet coefficients. With each sub-domain, we associate a rectangular matrix, $R_{\{ai,0\}\{j,\delta\}}{}^t$ of size $N \times n_{\{ai,0\}\{j,\delta\}}$. This matrix is the extension by $N_w - n_{\{ai,0\}\{j,\delta\}}$ counts of zeros to a vector x of size $n_{\{ai,0\}\{j,\delta\}}$ that belongs to $H_{\{ai,0\}\{j,\delta\}}$. Its elements are thus 1 or 0. The transpose of this matrix is the restriction matrix to sub-domain $H_{\{ai,0\}\{j,\delta\}}$. It acts on a vector of size N_w, and projects it on $H_{\{ai,0\}\{j,\delta\}}$ by holding only the entries that belong to $H_{\{ai,0\}\{j,\delta\}}$. We also define restricted extension operators by:

$$\hat{R}_{\{ai,0\},\{j,\delta\}}{}^t = R_{\{ai,0\}\{j,0\}}{}^t \cdot R_{\{ai,0\}\{j,0\}} \cdot R_{\{ai,0\}\{j,\delta\}}{}^t$$

Matrix $\hat{R}_{\{ai,0\}\{j,\delta\}}{}^t$ acts on a vector $x_{\{ai,0\}\{j,\delta\}}$ of size $n_{\{ai,0\}\{j,\delta\}}$ that belongs to $H_{\{ai,0\}\{j,\delta\}}$, projects it on non-overlapping sub-domain $H_{\{ai,0\}\{j,0\}}$ by eliminating all elements in the overlap area, and extends it by adding zeros to a vector x of size N_w. Finally, it is also possible to apply weights when extending vectors from $H_{\{ai,0\}\{j,\delta\}}$ to H, leading to a weighted, restricted extension operator:

$$\tilde{R}_{\{ai,0\}\{j,\delta\}}{}^t = w \cdot R_{\{ai,0\}\{j,0\}}{}^t \cdot R_{\{ai,0\}\{j,0\}} \cdot R_{\{ai,0\}\{j,\delta\}}{}^t$$

where $w(p)$ is the inverse of the number of overlapping blocks to which the p-th entry of $x_{\{ai,0\}\{j,\delta\}}$ belongs (it corresponds to the redundancy of the computation due to overlap). Now, instead of solving the normal system directly by projecting the data on H, we will project them on the sub-domains, derive partial sub-domain solutions involving a part of the wavelet coefficient vector x, and progressively build the global solution x by iterating the process. Such iterative algorithms are known as Schwarz algorithms.

3.2 Principle of the Schwarz algorithms

Let us start with the non-regularized case, where the normal system to solve is: $N \cdot x = f$.

The projection of the normal matrix N on sub-domain $H_{\{ai,0\}\{j,\delta\}}$ reads:

$$N_{\{ai,0\}\{j,\delta\}} = R_{\{ai,0\}\{j,\delta\}} \cdot N \cdot R_{\{ai,0\}\{j,\delta\}}{}^t$$

It is actually a block of N, comprising the entries related to the wavelets generating sub-space $H_{\{ai,0\}\{j,\delta\}}$.

Starting from an initial guess of the solution, we build a sequence of estimate $x^{k+1} = x^k + M \cdot (f - N \cdot x^k)$. In the parallel (additive) version of the algorithm, matrix M is:

$$M = \sum_{i=1}^{Nscales} \sum_{j=1}^{Nblocks(i)} \tilde{R}_{\{ai,0\}\{j,\delta\}}{}^t \cdot N_{\{ai,0\}\{j,\delta\}}{}^{-1} \cdot R_{\{ai,0\}\{j,\delta\}}$$

In other words, we first project the right hand side on $H_{\{ai,0\}\{j,\delta\}}$ and update it from previous estimates of solution:

$$f_{\{ai,0\}\{j,\delta\}}{}^k = R_{\{ai,0\}\{j,\delta\}} \cdot (f - R_{\{ai,0\}\{j,\delta\}} \cdot N \cdot x^k)$$

Note that the update matrix $R_{\{ai,0\}\{j,\delta\}} \cdot N$ is actually a band of N. Then, we solve the problem locally:

$$N_{\{ai,0\}\{j,\delta\}} \cdot x_{\{a_i,0\}\{j,\delta\}}{}^{k+1} = f_{\{ai,0\}\{j,\delta\}}{}^k$$

The last step is to extend the obtained coefficient vector $x_{\{ai,0\}\{j,\delta\}}{}^{k+1}$ to the full size N_w:

$$Ext\,[\,x_{\{ai,0\}\{j,\delta\}}{}^{k+1}] = \tilde{R}_{\{ai,0\}\{j,\delta\}}{}^t \cdot x_{\{ai,0\}\{j,\delta\}}{}^{k+1}.$$

At the end of the $(k+1)$-th iteration, we add all extended sub-domain solutions $Ext\ [x_{\{ai,0\}\{j,\delta\}}{}^{k+1}]$ to derive the global vector x^{k+1}, and we iterate the process.

In this version of the algorithm, all sub-domains are computed simultaneously, the global solution x^{k+1} being updated only after all $(k+1)$-th iterations of the local solution end. This parallel (also called additive) version of the algorithm converges more slowly than the sequential version (also called multiplicative), in which the global solution x^{k+1} is updated immediately after a sub-domain solution $x_{\{ai,0\}\{j,\delta\}}{}^{k+1}$ becomes available, and the $(k+1)$-th iteration of the next sub-domain solution is computed only after the global solution has been updated.

It is interesting to mix parallel iterations with sequential ones to find a hybrid algorithm with good convergence and parallelization properties. We thus carry out sequential iterations over the scale sub-domains and on a given scale we carry out parallel iterations over the blocks. This is the reason why we do not use overlapping scale sub-domains, but make use of overlapping blocks. The overlap speeds up the convergence in the parallel iterations, which converge more slowly, whereas the sequential iterations over scales, which converge faster, can be carried out without overlap.

Such a method will converge quickly if the sub-domains are not too correlated, reflecting the sparse structure of the normal matrix. In the case of wavelets that are well localized in both space and frequency, matrix N is sparse and, therefore it is quite appropriate for a hybrid algorithm to be used. Wavelets with different scales and positions are indeed not correlated too much.

Finally, there are many ways to iterate sequentially over the scales, which lead to more or less fast convergence. Fig. 2 shows the most widely used iteration sequences of the multi-level iterative approximation schemes called multigrid methods. Multigrid methods (Wesseling, 1991) are based on the resolution of successive projections of the normal system on coarse or fine grids, applying multi-level Schwarz iterations between sub-domains corresponding to the grids. In that respect, they are rather similar to a multi-scale resolution using wavelets. Consequently, we can design iteration schemes over the wavelet scales following the classical V-, W- and FMG-cycle iteration schemes of the multigrid algorithms.

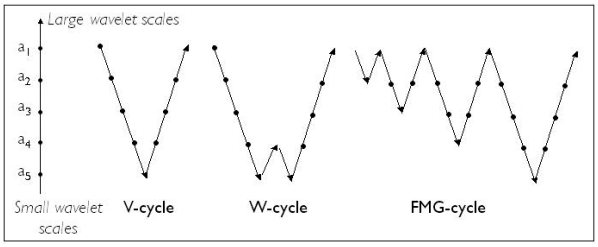

Fig. 2 Iteration schemes over the wavelet scales: V-cycle, W-cycle and FMG-cycle.

3.3 Approximations of the sub-domain normals

As we progressively refine our solution during the iteration process, we do not need to use exact sub-domain normal matrices at the beginning of the process, but apply adequate approximations to the sub-domain normals. For that, we follow the approach by Minchev *et al.* (2008). We construct a three-dimensional (3D), spherical tiling of the space on and outside of the Earth's sphere and approximate locally the values of the wavelets within each elementary tile, also called a 'cell' in the following. The 3D tiling is based on a spherical mesh and its radial extension. The 3D space is divided into radial layers of triangular prism cells sectioned by this mesh, so that the cells are neither too elongated nor too flat. The spherical mesh is derived by subdividing the facets of a regular icosahedron with respect to the sphere. For more details about this construction, the reader is referred to Chambodut *et al.* (2005). We obtain a very regular tiling with no singularity at the poles. Depending on the level of subdivision, one may obtain different level of fineness of the mesh.

There are different ways to approximate the wavelets locally within the cells. One may consider 3D Taylor series development at varying orders with different precision of approximation or simple averaging. The use of order-0 development or averaging actually projects the normal system on a 3D-grid and can be viewed as data filtering in the cell. Then, the precision of approximation should be adjusted depending on the wavelet scale to be computed. On each scale, we associate a mesh at a resolution similar to the wavelet scale.

As we progress in iteration, we gradually refine the

approximations of the sub-domain normals at all scales. Namely, as the sub-domain solutions at finer and finer scales become available, the solutions at the coarser scales have to be updated on a precision level compatible with the desired precision of the overall solution.

3.4 Scale-dependent reweighting to data

If the noise of the data is white, the weight associated with the data is the same on all scales and the weight matrix W_i is equal to $\alpha_i I$. However, this is not always fully realistic and we may need to consider a colored noise model. Let us suppose that matrix W_i is expressed in a quadratic form $C(r, r_1)$ with a colored spectral behaviour corresponding to the inverse of the power spectral density of the noise:

$$C(r, r_1) = \Sigma_l c_l P_l(r \cdot r_1)$$

where P_l is the Legendre polynomial of degree l and r and r_1 are two point vectors on the Earth's surface. Then, the normal matrices N_i are the discrete scalar products of the wavelets with the scalar product defined by this quadratic form. Assuming the quality of different datasets varies with different wavelength-bands, the normal matrix can be written in a very rough way by using scale-dependent constant weights. This allows us to accomplish a spectral combination of the datasets with rough consideration of their various spectral error characteristics.

3.5 The regularization

The algorithm may be directly applied to the regularized normal system. However, in the case of handling a large number of blocks and wavelet coefficients, the condition number of the normal matrix should be small enough in order for the solution to converge fast. This may require increasing the weight of the regularization matrix especially for high-resolution surface datasets, more than what one expects. Consequently, we choose to apply an iterated regularization approach (Engl, 1987). In such an approach, the regularized normals $G \cdot x = f$ are solved for the sub-domains, but the right hand side is updated by using the non-regularized normals N. This is equivalent to a progressive removal of the initial regularization as the iteration continues, the regularization being finally controlled by the number of iterations.

4. Validation with synthetic data

4.1 White noise case

We first validate this approach with synthetic data over Japan. Two sets of synthetic data are prepared for that purpose.

The first one is a set of gravity potential values as given by EGM2008 (Pavlis *et al.*, 2008), up to complete degree 120 (~170 km resolution): 5448 synthetic data on the ground level regularly distributed in the area between latitudes 27°N to 47°N and longitudes 131°E to 151°E. White noises (RMS = 1 m^2/s^2) are added. This noise level is a little lower than that of the satellite-only geopotential models as given by their error spectra up to degree/order 120.

The second dataset is a 3 by 3 minute grid of 103,041 free-air gravity anomalies on the ground level, also computed from EGM2008, over the area between latitudes 29°N to 45°N, and longitudes 133°E to 149°E. The resolution of this grid (5.5 km) corresponds to typical resolutions of surface gravity data and, accordingly, we can validate the approach under realistic situations. However, in order to simplify our test, the grid gravity anomalies are smoothed by truncating EGM2008 to degree 1000, and by applying damping starting at degree 730 with a half amplitude at degree 835. This corresponds to a spatial resolution of about 24 km. Finally, white noise is added to the dataset. At the resolution of the computed wavelet model (about 15 km), the amplitude of the noise is 0.35 mGals. As mentioned above, the low-frequency components of EGM2008 have been removed from both datasets. Fig. 3 shows the geographical distribution of the synthetic data.

The wavelet frame used is composed of five levels of scales as given in Table 1. Scales of the wavelets are about 300, 150, 75, 38 and 20 km, corresponding to the depths of the equivalent multipolar sources below a sphere of radius 6370 km, the average Earth radius. Because of the ellipticity, the depths with respect to the Earth's ellipsoid vary in a range of ± 3 km in the studied area, modifying slightly the wavelet scales on the ground level. Although the finest scale of the wavelets is 20 km, the wavelets can capture signal down to about 15 km resolution, because of the smooth

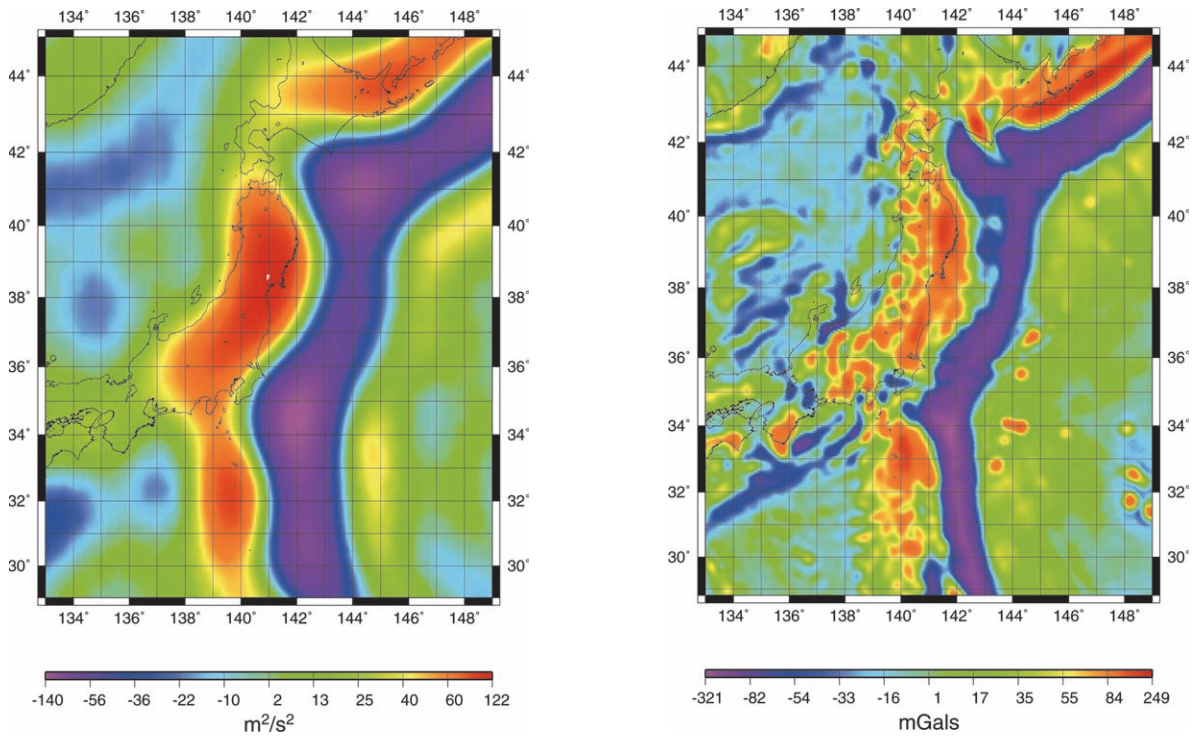

Fig. 3 Geographic distribution of the synthetic data. Left panel: potential data; *Right panel*: gravity anomaly data.

Table 1 Scales of wavelets in wavelet frames used in local modelling

Level	Scale (dimensionless)	Spatial scale (km)	Number of wavelets	Area covered
6	0.046875	300	380	25/49°N, 129/153°E
7	0.023438	150	1406	25/49°N, 129/153°E
8	0.011719	75	2401	29/45°N, 133/149°E
9	0.005859	38	9604	29/45°N, 133/149°E
10	0.0029297	20	38220	29/45°N, 133/149°E

decay of their spectrum. Finally, let us underline that, in the preparation of the synthetic potential data, we truncate EGM2008 at degree 120. Accordingly, we should also truncate the spherical harmonics expansion of the wavelets at the same degree for consistency. On the other hand, the anomaly data are treated as real observations independent of the potential data (though we apply a damping at the highest degrees to reduce the aliasing effects in the analysis). Therefore, we do not need to truncate the harmonics expansion of the wavelets in the construction of the gravity anomalies observation equations.

On levels 8, 9 and 10, the area is divided into 4, 16 and 36 blocks, respectively, and the computation of the wavelet coefficients are made in each block. Regarding the iteration scheme, we first test one FMG-cycle. At each step of the cycle the data are reduced in cells at a resolution corresponding to the finest wavelet scale that has been already computed.

Next, we apply about 40 V-cycles without any data reduction. On the finest scale, the total number of cells exceeds slightly the number of data themselves and, consequently, the projection of the data on the sub-domain becomes meaningless. On each scale, the number of block iterations ranges from a few tens to a few hundreds when there is more than one block. The weights to the data are given homogenously in space according to the noise level. In the spectral domain, larger weights are assigned to the geopotential data at the largest scales and to the anomaly data at the smaller scales. Wavelet coefficients from each of the two data sets are combined to yield a final wavelet model using the group redundancy numbers of the associated sub-domain normals (Schwintzer, 1990; Ilk *et al*., 2002).

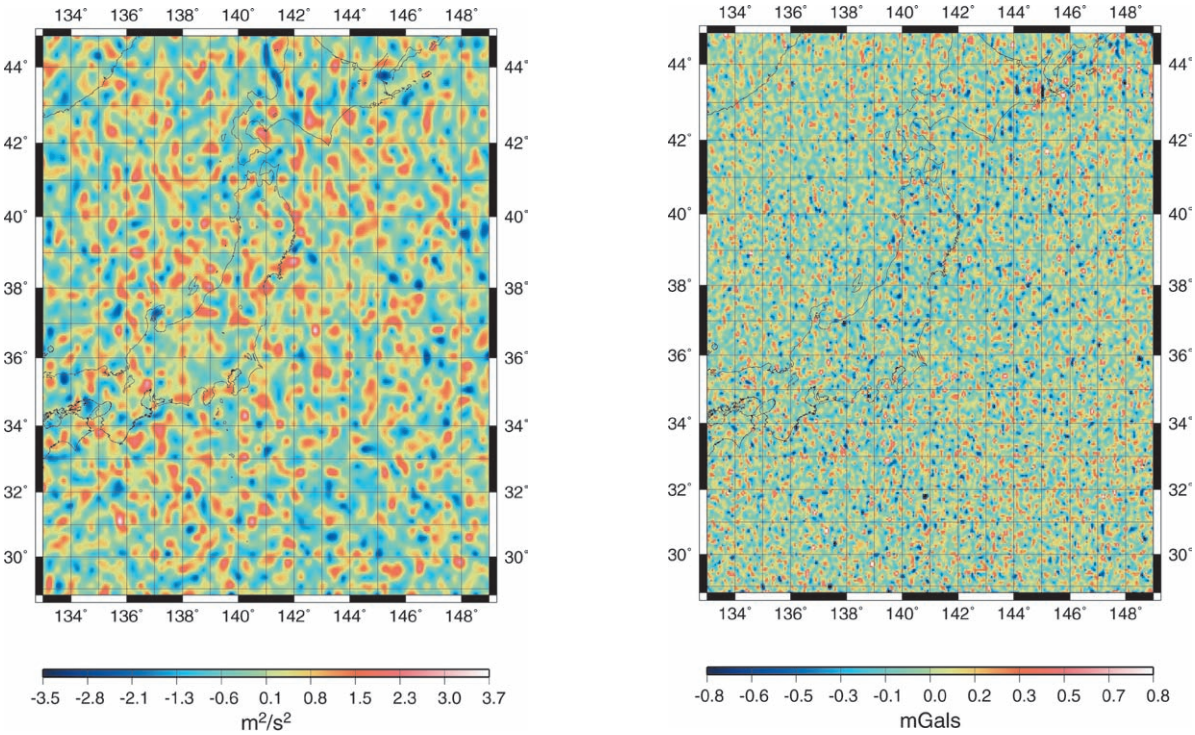

Fig. 4 Geographic distribution of residuals of the synthetic data. *Left panel*: potential residuals to degree 120. *Right panel*: gravity anomalies residuals at 15 km resolution.

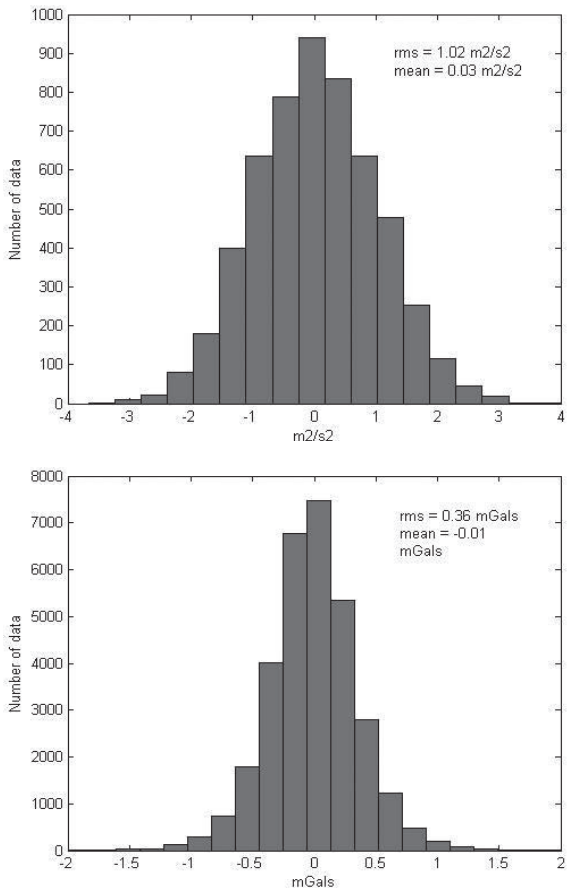

Fig. 5 Histograms of residuals of the respective synthetic data.

Top panel: potential residuals at degree 120.

Bottom panel: gravity anomalies residuals.

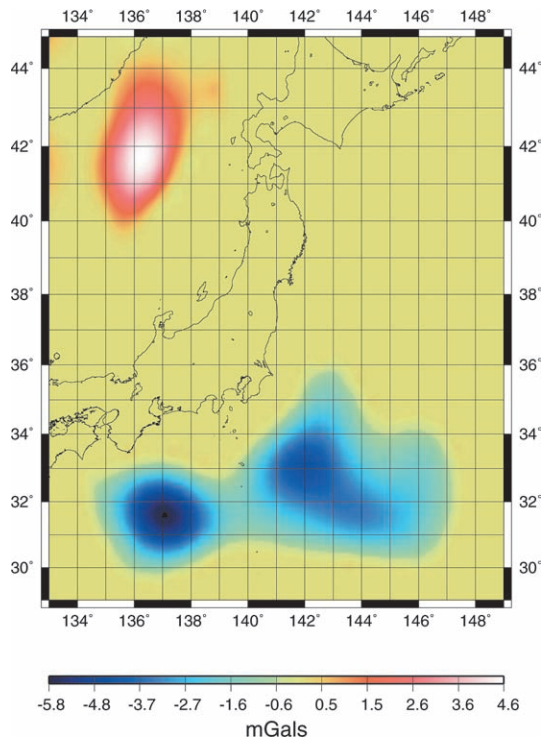

Fig. 6 Colored noise added to the gravity anomaly data.

The residuals of the respective data sets are shown geographically in Fig. 4 and their histograms are given in Fig. 5. The RMSs of residuals as in Fig. 5 are well restored to the applied noise levels and indicate a good performance in iteration: 1.02 m^2/s^2 with an average of 0.03 m^2/s^2 for the potential data, and 0.36 mGals with an average of 0.01 mGals for the gravity anomaly data. The spatial pattern of the residuals seems to be that of white noise in both the potential and gravity anomaly data.

Only slightly noticeable is the feature with a larger amplitude around east Hokkaido, where EGM2008 (and the actual gravity field) contains strong signals at high frequencies. During the iteration process we learn that the residuals there show a small, but systematic trend of some 0.05 mGals in amplitude at earlier stages of iteration, but such a trend has gradually disappeared as iteration goes.

4.2 Colored noise case

As a second validation with synthetic data, we assume the existence of realistic systematic errors as colored noise in the anomaly data. Such types of errors may exist near the coasts in altimetry-derived gravity anomalies or in ship-borne gravity surveys. Then, we additionally append such errors as shown in Fig. 6 to the free-air gravity anomaly data, but we do not modify the potential data, both obtained in the preceding section. The same analysis as that in the previous section is carried out on these data.

After completion of the one FMG-cycle iteration, the residuals of the respective data are shown geographically in Fig. 7. Notable patterns at large scales are found correspondingly to the location of the colored noise. The spatial pattern of the residuals of the gravity anomaly data looks smoother than that of the appended noise, whereas the residuals of the potential data seem to contain smaller scale components of the original noise. This reflects the difference in the spectral weight assignment to the two datasets. On the largest scale almost no weight is given to the gravity anomaly data and large residuals should appear in the anomaly data, whereas on wavelet scales 150 km or smaller, larger weights are provided to the anomaly data and larger residuals should come out in the potential data.

To improve the hybrid model, we try to apply downweights to the gravity anomaly data based on the map of the smoothed residuals. The resulting weight

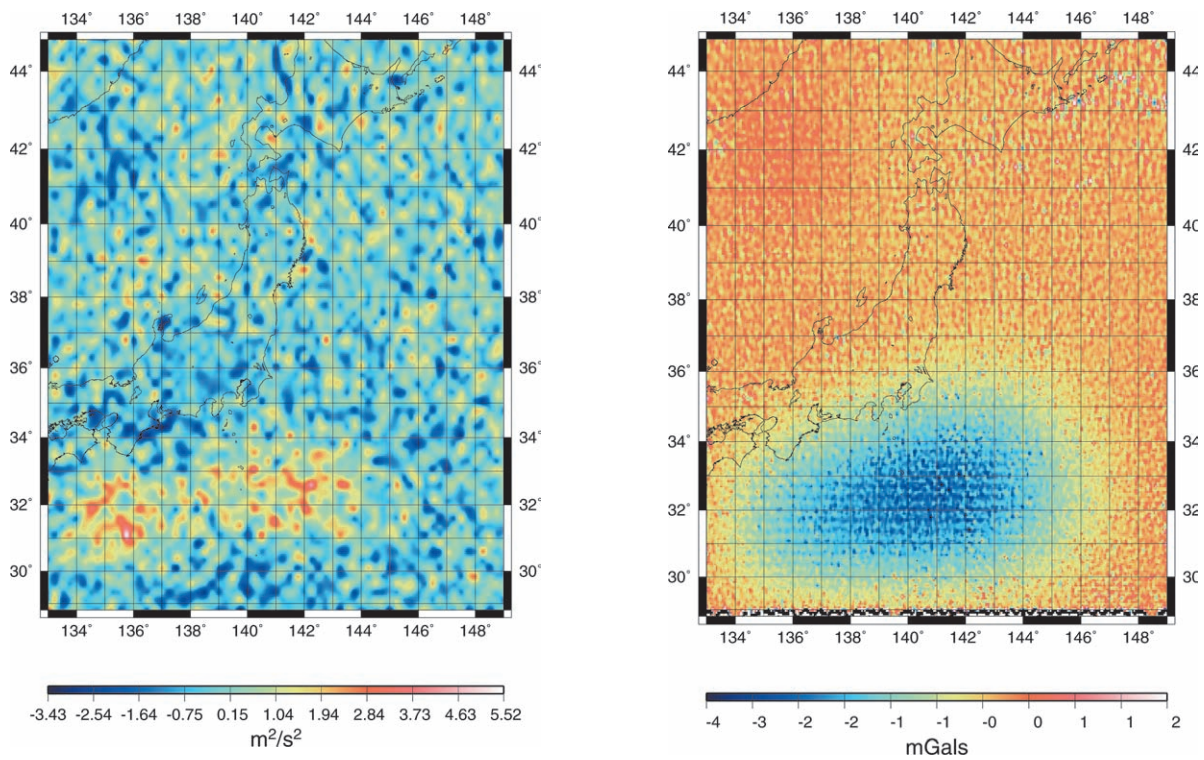

Fig. 7 Geographical distribution of residuals of the synthetic data. *Left panel*: potential residuals up to degree 120. *Right panel*: gravity anomalies at 15 km resolution.

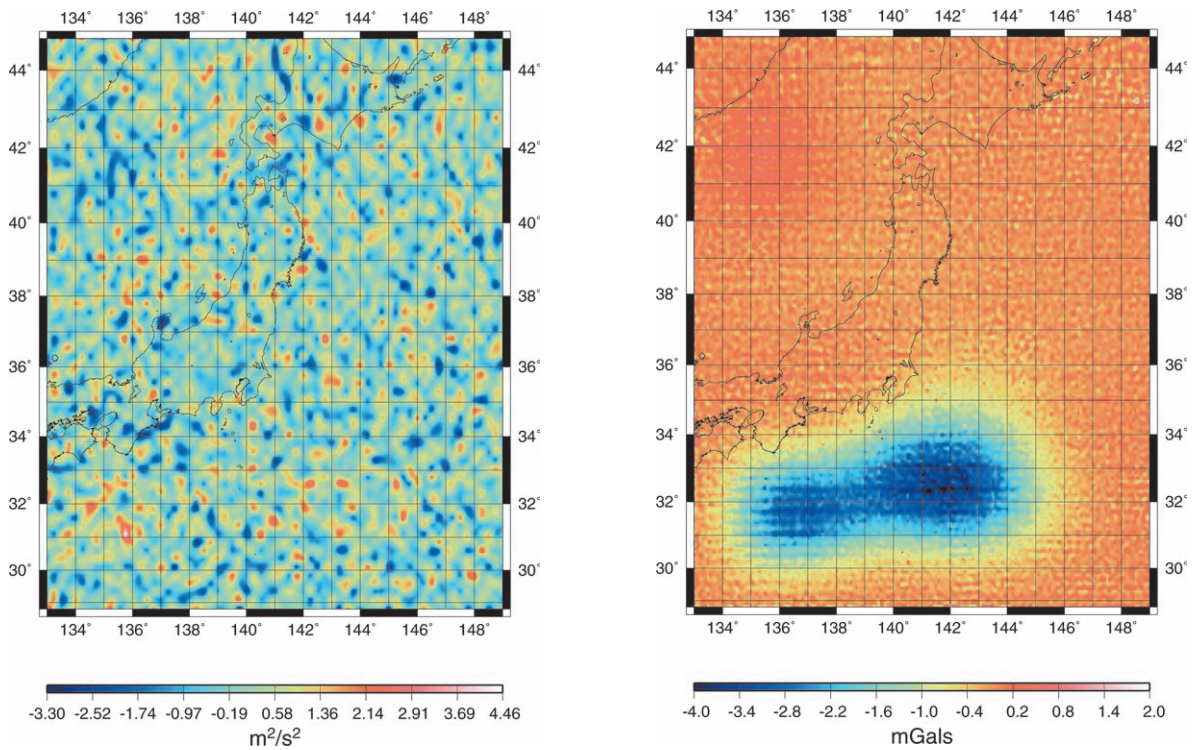

Fig. 8 Geographical distribution of residuals of the synthetic data after applying downweights to the anomaly data. *Left panel*: potential residuals up to degree 120. *Right panel*: gravity anomalies at 15 km resolution.

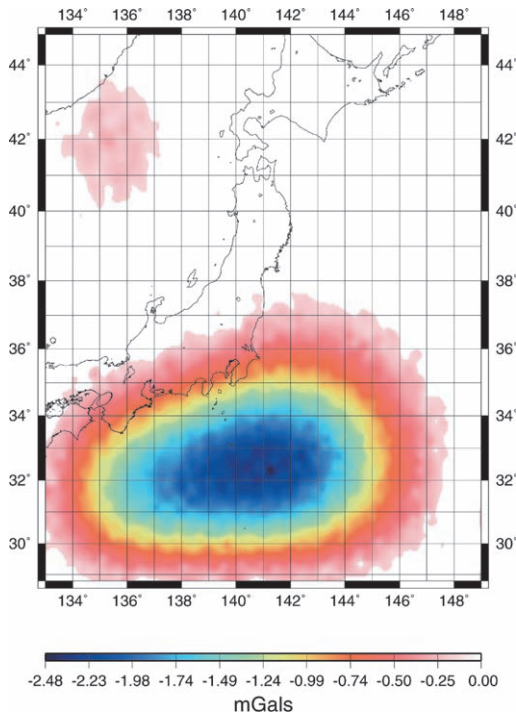

Fig. 9 Downweighting to the gravity anomaly dataset.

reduction model is shown in Fig. 9. By using the downweight model thus obtained, we perform two more V-cycles of iteration.

Fig. 8 displays the geographical distribution of the residuals of the two data sets. We observe no clear pattern in the residuals of the potential data, but a pattern of white noise. The RMS of the residuals is compatible to the level of the assumed white noise. The residuals of the gravity anomaly data become less smooth than that of Fig. 7, and much closer to the pattern of the appended noise as in Fig. 6. This indicates the effectiveness of downweighting in the reduction of error contamination in the combined model derived if the residuals are identified to attribute to systematic errors. We conclude, therefore, that our choice of weights was reasonable, leading to a fairly good model given the synthetic data characteristics, and that the method developed is valid for local gravity field modeling from different sets of data with different error characteristics.

Note that increase in weights at intermediate scales of the potential data did not improve the resulting model. At those scales the anomaly data contain reliable signals, but are assigned to smaller weights, leading to adjust (worsen) the anomaly data fitted to the pattern, if any, of white noise in the potential data.

It is important to recognize that the pattern of the gravity anomaly residuals does not perfectly reproduce